International Journal of Scientific Engineering and Applied Science (IJSEAS) – Volume-8, Issue-7, July 2022
ISSN: 2395-3470
www.ijseas.com

Darcy-Forchheimer Flow on Variable Thermal Conductivity, Heat Source, and Suction/Injection in Channels: Numerical Therapy

[1]Hussaini Abdullahi1, [2]Ahmad Rufai, [3]Sadiq Shehu
[1,2,3]Department of Mathematics, Sokoto State University, Sokoto, Nigeria.

Abstract
This holograph addresses the effects of Darcy-Forchheimer flow of hydromagnetic viscous incompressible fluid in a vertical infinite porous channel. The governing equations in dimensionless form is considered to the analysis. Implicit-finite difference scheme is employed to obtain the numerical solutions of the non-linear differential equations governing the flow. Relevance fluid flow quantities are found and portrayed graphically. Also, skin-friction, Nusselt number, and Sherwood number are obtained and presented in tabular form. It is understood that velocity, temperature, and concentration of the fluid change substantially with Forchheimer parameter, variable viscosity parameter, thermal conductivity parameter, and chemical reaction parameter.
Keywords: Power-law fluid, non-Newtonian fluid, implicit technique, variable thermal conductivity.

1. Introduction

Numerous articles [1–6] on the boundary layer flow of non-Newtonian fluids have been published in the fields of chemical engineering and fluid mechanics. The rheological equation of state between shear stress and strain rate tensor is given by for one of the fluids with the most practical significance, the power-law fluid.

$$\tau_{yx} = -m\left|\frac{\partial u}{\partial y}\right|^{n-1}\frac{\partial u}{\partial y}$$

When n = 1, a fluid has a dynamic coefficient of viscosity of m and is Newtonian; when n > 1, a fluid is dilatant; and when n = 1, a fluid is pseudo-plastic. Researchers and scientists have recently become interested in non-Newtonian fluid flow, particularly the power-law model, because of its applications in the food, polymer, petroleum-chemical, geothermal, rubber, paint, and biological industries, see [1].

MHD flow and non-Newtonian fluid behaviour issues have recently become crucial due to their widespread use in industrial manufacturing processes like plasma studies and the petroleum sector, aerodynamic boundary layer control and magnetohydrodynamic cooling of transparent reactors. The effects of magnetic fields on mixed, natural, and forced convection heat and mass transfer in non-Newtonian fluids have been extensively researched. Many academics have been interested in magnetohydrodynamics because of its many uses. It is used to research star and solar structures, interstellar materials, radio transmission through the ionosphere, and other topics in astrophysics and geophysics. It is used in engineering in MHD pumps, MHD bearings, etc. Convection of non-Newtonian fluid through a porous medium has uses in the extraction of oil, the storage of thermal energy, and the flow through filters. The theory of stellar structure also frequently discusses the phenomenon of mass transfer, and its consequences can be seen, at least on the solar surface. In liquid metals, electrolytes, and ionised gases, the study of the effects of magnetic fields on the free convection movement of non-Newtonian fluids is crucial. In power engineering and metallurgy, the thermal physics of hydromagnetic problems with mass transport is of importance. The magnetohydrodynamic flow of a power law fluid model toward a stretching sheet was studied by Anderson et al. [7]. By taking into account suction/injection and magnetic field effects, Chen [8] examined the heat transfer phenomena of a non-Newtonian power law fluid over a porous stretched sheet. Chaitanya and Dhiman [9] conducted a thorough investigation into the flow and heat transfer of a non-Newtonian power law fluid in two adjacent circular cylinders. Sui et al. [10] recently discussed the mixed convective heat transfer for power law fluids along an inclined plate over a moving conveyor. When high temperatures are involved, such as in the storage of thermal energy, gas turbines, nuclear power plants, etc., convective heat transfer is of great interest. It is well known that because of numerous important applications, including geothermal energy extraction, material fading, solid matrix or micro porous heat exchangers, micro thrusters, etc., convective boundary conditions have been extensively researched experimentally and numerically. Due to the convective boundary conditions' practical significance, various authors have looked into their studies on the subject. The heat transport of a viscous fluid over a stretching/shrinking sheet with convective boundary conditions was described by Yao et al. [11]. The MHD mixed convection heat transmission in a porous medium over a vertically convicted heated plate was presented by Makinde and Aziz [12]. By taking into account the

convective boundary circumstances, Khan et al. [13] explored the mixed convective heat transfer in Sisko fluid towards a radially extending sheet. Mahanta and Shaw [14] reported on the 3D Casson fluid flow that passed through a porous linearly stretched sheet. The steady flow and heat transfer in an Eyring Powell fluid over a continuously moving plate with convective boundary conditions were examined by Hayat et al. [15]. Shahzad and Ali [16] studied the effect of convective boundary conditions on the magnetohydrodynamic flow of a power law fluid across a vertical stretched sheet.

Numerous engineering and scientific domains have significant applications for fluid flows via porous media. Due to the various types of unique rock and soil with varied porosities where subsurface flows occur, it is, for instance, extremely important in geomechanics. Petroleum engineering and hydrogeology are appropriate examples. Applications of the latter include groundwater modelling, soil drainage, modelling of soil contamination by contaminants, and underground storage of nuclear waste. Regarding petroleum engineering, there is a great need for effective extraction methods due to the rising demand for oil. As a result, sophisticated modelling techniques for better oil recovery, which demonstrate non-Newtonian properties, are also required. Because non-Newtonian fluids, like blood, exist, biological engineering provides additional significant instances of non-Newtonian flows in porous media. Numerous pertinent engineering applications, such as the flow of perforation mud in oil wells and porous bearing lubrication, involve flows of non-Newtonian fluids in ducts with permeable walls. In some circumstances, it might be particularly useful to examine non-Newtonian fluid flow in a channel that is partially filled with a porous medium. For instance, a wide range of fluids employed in oil field applications display non-Newtonian behaviour across a certain range of shear rates, such as power-law-like behaviour [17].

The properties of the final product heavily depend on the rate of cooling involved in modern metallurgical and metal-working processes like drawing continuous filaments through quiescent fluids and annealing and tinning copper wires, which all involve the study of magnetohydrodynamic (MHD) flow of an electrically conducting fluid. Due to its applicability to a variety of technical issues, including MHD generators, nuclear reactors, and geothermal energy extraction, this form of flow has also drawn the attention of numerous researchers. The impact of the transverse magnetic field on the boundary-layer flow characteristics has been studied in great detail. By accounting for the magnetic field, Vajravelu and Rollins [18] investigated heat transport in an electrically conducting fluid over a stretching surface. The MHD flow of a viscoelastic fluid through a porous medium between infinite parallel plates with time-dependent suction was investigated by Baag et al. [19]. The Oldroyd-B type non-Newtonian fluid in a wedge with a non-uniform heat source and sink was studied by Reddy et al. [20]. Gireesha and his colleagues [21, 22] have investigated how different flow phenomena are influenced by factors such as buoyancy, heat radiation, chemical reaction, and more. Additionally, Mahanthesh and his colleagues' research on heat transfer phenomena where the flow through a stretched surface has been established [19–21].

In light of the aforementioned debates, the current work examines the impact of thermal conductivity on a power-law fluid in an infinite vertical plate while heat dissipation and an uneven source/sink of heat are present. A transverse magnetic field parallel to the plate is applied to the flow. The fluid flow in the porous medium is described using the Forchheimer extension. Equations involving the transmission of highly nonlinear momentum and heat are quantitatively solved using the implicit finite difference method. Graphs of the impacts of several parameters on the concentration, temperature, and velocity profiles are shown. It is intended that the findings of the current analysis will complement earlier research and offer practical knowledge for application.

2. Formulation of the Problem

Conceive the natural convection heat and mass transfer past an infinite vertical plate in a non-Newtonian power-law fluid saturated Darcy porous medium. Assume the coordinate system such that x-axis is by the vertical plate and y-axis normal to the plate. The plates are held at variable surface temperature and concentration, T_w, and C_w respectively. The temperature and concentration of the ambient medium are T_h and C_h severally. Presume that the fluid and the porous medium have constant physical properties except for the density variation required by the Boussinesq approximation. The flow is unsteady, laminar, two dimensional. The porous medium is isotropic and homogeneous. The fluid and the porous medium are in local thermodynamical equilibrium. In addition, the Soret and Dufour effects are taken into consideration. Under these conditions, the governing equations describing the fluid flow can be written as follows:

International Journal of Scientific Engineering and Applied Science (IJSEAS) – Volume-8, Issue-7, July 2022
ISSN: 2395-3470
www.ijseas.com

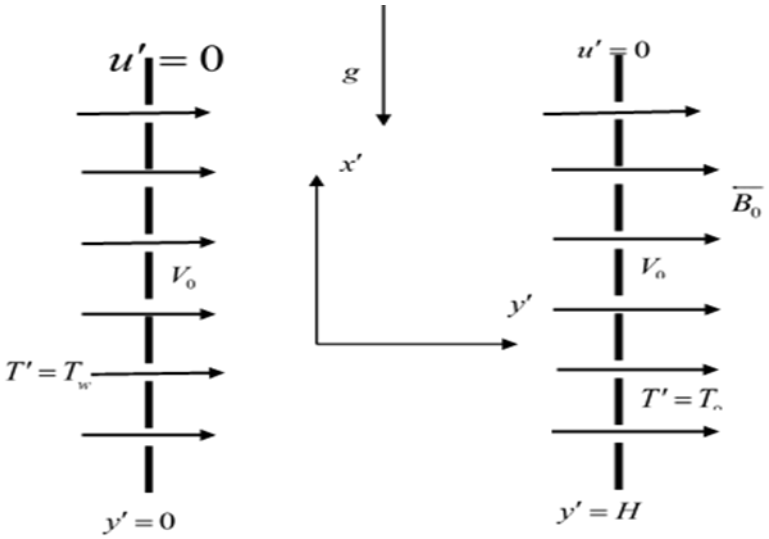

Figure 1: Geometry instituting the problem

5The Continuity Equation:

$$\frac{\partial v}{\partial y}=0 \tag{1}$$

The Momentum

Equation: $$\frac{\partial u'}{\partial t'}+v'\frac{\partial u'}{\partial y'}=\left\{\frac{\mu_0}{\rho}\frac{\partial}{\partial y'}\left[e^{-\lambda(T'-T_h')}\frac{\partial u'}{\partial y'}\right]\right\}^{n-1}+g\beta\left(T'-T_h'\right)+g\beta^*\left(C'-C_h'\right)-\frac{\sigma B_0^2}{\rho}u'-\frac{\upsilon}{k'}u' \tag{2}$$

The Energy Equation

$$\frac{\partial T'}{\partial t'}+v'\frac{\partial T'}{\partial y'}=\frac{k_0}{\rho c_p}\frac{\partial}{\partial y'}\left\{(1+\gamma)\frac{\partial T'}{\partial y'}\right\}+\frac{QC_0^{\bullet}A}{\rho c_p}\exp\left(\frac{-E}{RT}\right)+\frac{\mu}{c_p}\left(\frac{\partial u'}{\partial y'}\right)^2+\frac{D_mK_T}{C_sC_p}\frac{\partial^2 C}{\partial y^2}+\frac{Q_0}{\rho C_P}\left(T'-T_h'\right)+b^*u'^2 \tag{3}$$

The Concentration Equation

$$\frac{\partial C'}{\partial t'}+v'\frac{\partial C'}{\partial y'}=D\frac{\partial^2 C'}{\partial y'^2}-R\left(C'-C_h'\right)^q+\frac{D_mK_T}{T_M}\frac{\partial^2 T'}{\partial y'^2} \tag{4}$$

The initial and boundary conditions are :

$$t'\le 0: u'=0, T'=T_0, C'=C_0 \text{ for } 0\le y'\le H$$

$$t'>0:\begin{cases}u'=0, T'=T_\omega, C'=C_\omega \text{ at } y'=0\\ u'=0, T'=T_0, C'=C_0 \text{ at } y'=H\end{cases} \tag{5}$$

Whereas u, v are the velocity components in x, y directions respectively, t' - the time, g – the acceleration due to gravity, β - the volumetric coefficient of thermal expansion, β^* - the volumetric coefficient of expansion with concentration, T' -the temperature of the fluid in the boundary layer, C' -the species concentration in the boundary layer, υ -the kinematic viscosity, σ -the electrical conductivity, B_0 -the magnetic induction, ρ -the density of the fluid, c_p -the specific heat at constant pressure, q_r -the radiation heat flux, Q_0 -the heat generation/absorption and D -the species diffusion coefficient, F^* -the Forchheimer parameter, b^* -the Hall current parameter.

For similarity result of the flow equations, we brought in the dimensionless variables defined as follows:

$$\left.\begin{aligned}
&x=\frac{x'}{H},\ y=\frac{y'}{H},\ u=\frac{u'}{U_o},\ T=\frac{T'-T_h'}{T_w-T_h},\ C=\frac{C'-C_h'}{C_w-C_h},\ t=\frac{U_o t'}{H}\\
&\Pr=\frac{\rho\upsilon Cp}{k},\ Sc=\frac{\upsilon}{D},\ Gr=\frac{g\beta_T\left(T_w'-T_h'\right)H}{U_0^2},\ Gm=\frac{g\beta_c\left(C_w'-C_h'\right)H}{U_0^2}\\
&M=\frac{\sigma B_0^2 H}{U_0\rho},\ Kr=\frac{KcH}{U_0},\ Ec=\frac{\mu U_0}{HCp\left(T_w'-T_h'\right)},\ T_1=\frac{E\left(T'-T_h\right)}{RT_h^2},\\
&\delta=\frac{QC_0^{\bullet}AEH^2}{RT_h^2}\exp\left(\frac{-E}{RT_h}\right),\ \varepsilon=\frac{RT_h}{E},\ Du=\frac{D_mK_T}{C_sCpU_0H}\frac{\left(C_w'-C_h'\right)}{\left(T_w'-T_h'\right)},\\
&Sr=\frac{D_mK_TH}{T_MU_0}\frac{\left(T_w'-T_h'\right)}{\left(C_w'-C_h'\right)}
\end{aligned}\right\} \tag{6}$$

Where $U_0=\left[\frac{\rho H^n}{k}\right]^{\frac{1}{n-2}}$ and H is the distance between the two plates. Integrating Eqn. (6) in Eqns. (2)-(5), the flow equations in new variable quantity concede

$$\frac{\partial u}{\partial t}+\eta\frac{\partial u}{\partial y}=\left\{\exp\left(-\lambda T\right)\left[\frac{\partial^2 u}{\partial y^2}-\lambda\frac{\partial u}{\partial y}\frac{\partial T}{\partial y}\right]\right\}^{n-1}+Gr\theta+GcC-\left(M+\frac{1}{Da\,\mathrm{Re}}\right)u \tag{7}$$

$$\Pr\left[\frac{\partial T}{\partial t}+\eta\frac{\partial T}{\partial y}\right]=\left\{1+\gamma T\right\}\frac{\partial^2 T}{\partial y^2}+\gamma\left(\frac{\partial T}{\partial y}\right)^2+\Pr Ec\left(\frac{\partial u}{\partial y}\right)^2+\Pr\delta\exp\left(\frac{T_1}{1+\varepsilon T}\right)+\Pr\phi T+\Pr Du\frac{\partial^2 C}{\partial y^2}+\Pr bu^2 \tag{8}$$

$$Sc\left[\frac{\partial C}{\partial t}+\eta\frac{\partial C}{\partial y}\right]=\frac{\partial^2 C}{\partial y^2}-ScKrC^n+ScSr\frac{\partial^2 T}{\partial y^2} \tag{9}$$

The initial and boundary conditions (5) in non-dimensional form are given by

$$t>0:\ \begin{cases}u=0, & \theta=1, C=1 \quad at\ \ y=0\\ u=0, & \theta=0, C=0 \quad at\ \ y=1\end{cases} \tag{10}$$

Where Gr is the Grashof number, Gc is the modified Grashof number, $\Pr$ is the Prandtl number. Sc is the Schmidt number, M is the Magnetic parameter, Ec is the Eckert number and Kr the chemical reaction parameter, λ is the variable viscosity parameter, Du is the Dufour number, Sr is the Soret number, γ is the thermal conductivity parameter, δ is the Frank-Kamenetskii parameter, and ε is the activation energy parameter.

The most substantial quantities of physical relevant with regards to engineering process are skin- friction coefficient, Nusselt number, and Sherwood number which are stated below from the computed velocity, temperature, and concentration field on the plates $y=0$ and $y=1$

$$C_f=\exp\left(-\lambda T\right)\left|\frac{\partial U}{\partial Y}\right|^{n-1}\left[\frac{\partial U}{\partial Y}\right]_{Y=0,1} \tag{11}$$

$$Nu_x=-\left(1+\gamma T\right)Gr^{1/4}\left[\frac{\partial T}{\partial Y}\right]_{Y=0,1} \tag{12}$$

$$Sh_x = \left(\frac{\partial C}{\partial y}\right)_{y=0,1} \tag{13}$$

3. Numerical Technique

The governing equations (7-9) are unsteady, coupled and non-linear with initial and boundary conditions (10). Using implicit finite-difference scheme given by Makinde and Chinyoka [27] employing MALAB software. Forward difference formulae are utilized for all time derivatives and approximated both the second and first derivatives with second order central differences to discretized the momentum, energy, and concentration equations into finite difference equations. The equations are transformed into a system of linear algebraic equations in the tridiagonal form as:

$$\left(1+\Delta tM+\frac{\Delta t}{Da\,\mathrm{Re}}\right)u_i^j = \Delta t\left(\frac{1}{\Delta y^2}\exp(-\lambda T_i^{\,j})(u_{i-1}^j-2u_i^j+u_{i+1}^j)-\frac{\lambda}{4\Delta y^2}\exp(-\lambda T_i^{\,j})(u_{i+1}^j-u_{i-1}^j)(T_{i+1}^j-T_{i-1}^j)\right)^{n-1} -$$

$$\eta r_3\left(u_{i+1}^j-u_i^j\right)u_{i+1}^j+u_i^j+\Delta tT_i^{\,j}+\Delta tNC_i^j+Fr(u_i^j)^2 \tag{14}$$

$$-r_1r_8T_{i-1}^{j+1}+\left(\mathrm{Pr}+2r_1r_8\right)T_i^{j+1}-r_1r_8T_{i+1}^{j+1}=r_2r_8T_{i-1}^j+\left(\mathrm{Pr}+\eta r_4\,\mathrm{Pr}-2r_2r_8+\Delta t\,\mathrm{Pr}\,\phi\right)T_i^j+$$

$$\left(r_2r_8-\eta r_4\,\mathrm{Pr}\right)T_{i+1}^j+r_3\,\mathrm{Pr}\,Ec\left(u_{i+1}^j-u_{i-1}^j\right)^2+r_3\gamma\left(T_{i+1}^j-T_{i-1}^j\right)^2+\ldots$$

$$\Delta t\delta\exp\left(\frac{(T_1)_i^j}{1+\varepsilon T_i^j}\right)+Du\frac{\Delta t}{\Delta y^2}(C_{i-1}^j-2C_i^j+C_{i+1}^j)+\left(u_i^j\right)b\Delta t \tag{15}$$

$$-r_1C_{i-1}^{j+1}+\left(Sc+2r_1\right)C_i^{j+1}-r_1C_{i-1}^{j+1}=r_2C_{i+1}^j+(Sc+\eta Scr_4-2r_2)C_i^j-\Delta tScKr(C_i^j)^q+$$

$$\left(r_2-\eta Scr_4\right)C_{i+1}^j+r_7\left(T_{i-1}^j-2T_i^{\,j}+T_{i+1}^j\right) \tag{16}$$

$$r_1=\frac{\alpha\Delta t}{\Delta y^2};\quad r_2=\frac{(1-\alpha)\Delta t}{\Delta y^2};\quad r_3=\frac{\Delta t}{4\Delta y^2};\quad r_4=\frac{\Delta t}{\Delta y};\quad r_8=1+\gamma T_i^{\,j}+\frac{4}{3F};0<\alpha<1.$$

For each time step, firstly the concentration and temperature fields have been solved, then using the already known values of the concentration and temperature fields the velocity field is evaluated. The process of computation is uninterrupted until a steady state is approached by satisfying the following convergence criterion

$$\frac{\sum\left|A_{i,j+1}-A_{i,j}\right|}{M\left|A\right|_{\max}}<10^{-5} \tag{17}$$

Here $A_{i,j}$ stands for the velocity or temperature fields, M is the number of interior grid points and $\left|A\right|_{\max}$ is the maximum absolute value of $A_{i,j}$.

4. Results and Discussion

We have formulated and addressed the issue of non-Newtonian power-law fluid MHD free convection flow across a vertical plate with variable thermal conductivity and suction/injection effects in the preceding sections. In this study, the default parameter values b=10.0, Fr=1.0, Gr=10.0, Gc=5.0, Du=0.1, γ =1.0, ϕ=1.0, δ =0.1, Ec=0.01, M=1.0, ε =0.01, Sc=0.23, and Kr=1.0 are used for computations. Thus, unless otherwise stated in the relevant graph, all graphs correspond to these values. The distribution of velocity, velocity/temperature, and velocity/concentration is shown in Figures 2–5, Figures 6–11, and Figures 12–14, respectively. Variations in skin friction, Nusselt number, and Sherwood number are shown in Tables (1-3).

As the magnetic field (M) intensity increases, we can see from Figure 2 that the velocity profiles decrease. This is because the introduction of a transverse magnetic field that is perpendicular to the flow direction has the propensity to produce the Lorentz force, a drag force that tends to resist the flow. The effects of the thermal Grashof number (Gr) on the velocity profile for fixed values of the other parameters are shown in Figure 3. It has been found that as Gr grows, the dimensionless velocity rises. Since the relative impact of thermal buoyant force to viscous hydrodynamic force in the boundary layer determines the Grashof

number for heat transfer. The impact of the changed Grashof number (Gm) on the dimensionless velocity profiles is seen in Figure 4. It is observed that the velocities rise as the mass Grashof number (Gm) rises. The ratio of a species' buoyant force to its viscous hydrodynamic force is theoretically defined by its mass Grashof number, or Gm. The improvement of species buoyant flow causes the velocity to grow as it rises. As the permeability parameter (K) is increased, the velocity also increases, as can be seen in Figure 5. The fluid speed is observable throughout the entire fluid region at a lower permeability.

Figure 6 shows how the Prandtl number (Pr) affects the velocity and temperature curves. According to the plot, the velocity falls as the Prandtl number (Pr) rises. This is due to the fact that the Prandtl number suggests that in the regime of the peripheral layer, momentum diffusion has a greater influence than heat diffusion. The momentum diffusion rate outperforms the thermal diffusion rate when the Prandtl number Pr=1. As a result, the Prandtl number will increase and the fluid regime's velocity will drop. Figure 6(b) shows that as the Prandtl number increases, the temperature decreases. This is caused by the relatively low thermal conductivity of a fluid with a high Prandtl number, which causes a reduction in the thickness of the thermal boundary layer. Figure 7 shows how the variable thermal conductivity parameter (γ) affects temperature and velocity profiles. It suggests that for various values of the variable thermal conductivity parameter (γ), the temperature as well as the velocity are reduced in the boundary layer. While keeping other parameters constant, Figure 8 illustrates how the Frank-Kamenetskii parameter (δ) varies on the velocity and temperature profiles. The numerical results demonstrate that as the Frank-Kamenetskii parameter (δ) is raised in both air $(\mathrm{Pr}=0.7)$ and water $(\mathrm{Pr}=7.1)$, both velocity and temperature rise. Figure 9 depicts the impact of the Eckert number on the temperature and velocity profiles of the two working fluids, air $(\mathrm{Pr}=0.7)$ and water $(\mathrm{Pr}=7.1)$. Because the Eckert number (Ec) expresses the relationship between kinetic energy in the flow and enthalpy, it is possible to conclude from Figure 9(a), that it has been noted that while the Eckert number increases in the air $(\mathrm{Pr}=0.7)$, it falls in the water $(\mathrm{Pr}=7.1)$. This is because the Eckert number symbolises the process through which labour against viscous fluid stresses converts kinetic energy into internal energy. Furthermore, Figure 9(b) shows that when the Eckert number changes, the temperature rises. For various values of the Dufour number (Du), the transient velocity and temperature profiles for air $(\mathrm{Pr}=0.7)$ and water $(\mathrm{Pr}=7.1)$ are displayed in Figure 10. It has been observed that an increase in the Dufour number causes an increase in both temperature and velocity. Figure 11 depicts the effect of the heat generation parameter (ϕ) on the dimensionless velocity and temperature for the fixed values of the other parameters. It is seen that the heat generation parameter (ϕ) causes an increase in both the dimensionless velocity and temperature profiles.

The impact of the chemical reaction parameter (Kr) on the velocity and concentration for fixed values of other parameters is shown in Fig. 12. It has been shown that as Kr increases, both velocity and concentration decrease. The Schmidt number (Sc) effect on velocity and concentration profiles is depicted in Fig. 13. The relative efficiency of momentum and mass transport by diffusion in velocity and concentration fields is defined by the Schmidt number. According to a comparison of the curves in the figure, when the Schmidt number (Sc) is raised, the velocity and concentration both drop. The outcome of the dimensionless velocity and concentration for various Soret parameter (Sr) values was shown in Figure 14. The figures make it quite evident that as density increases, so do the velocity and concentration profiles.

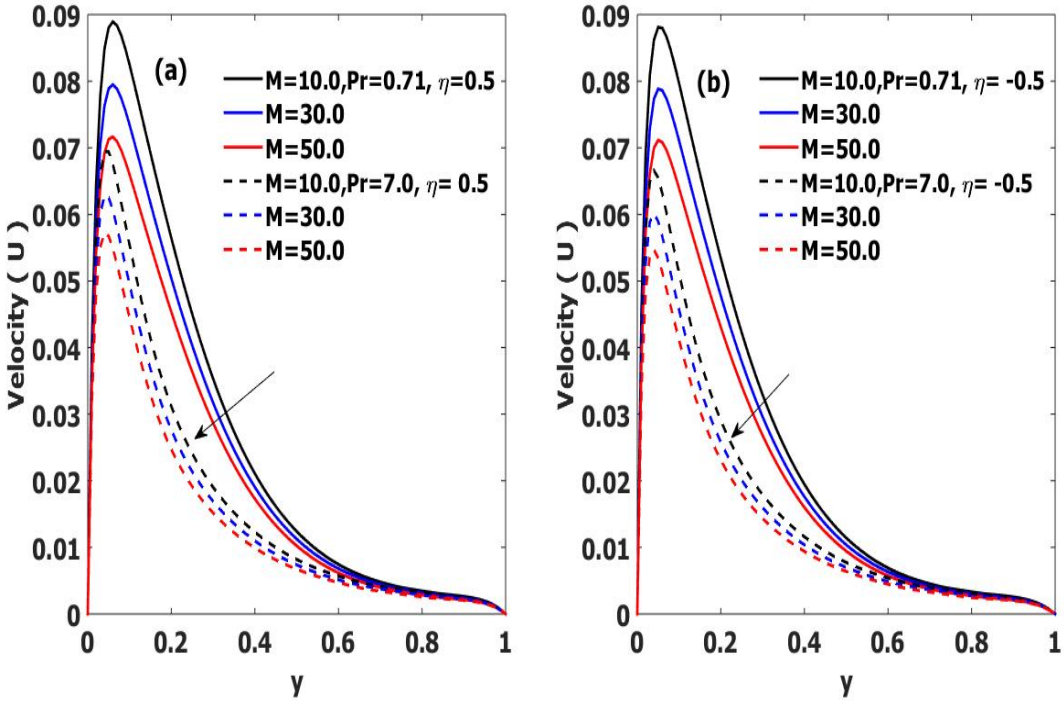

Figure 2: Influence of M on velocity profiles

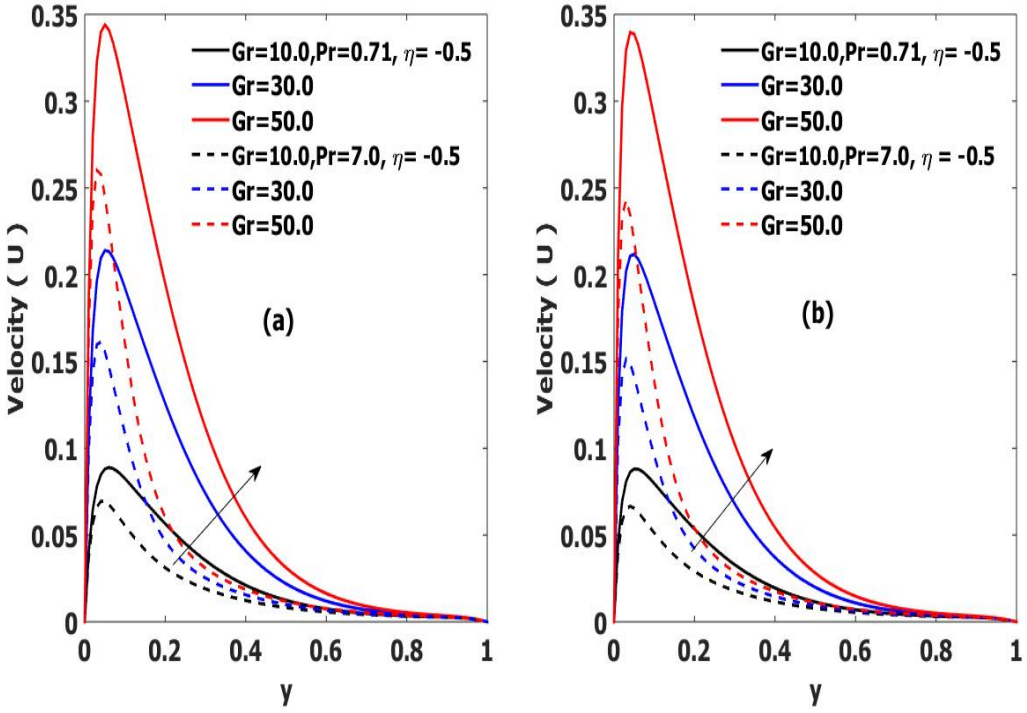

Figure 3: Influence of Gr on velocity profiles

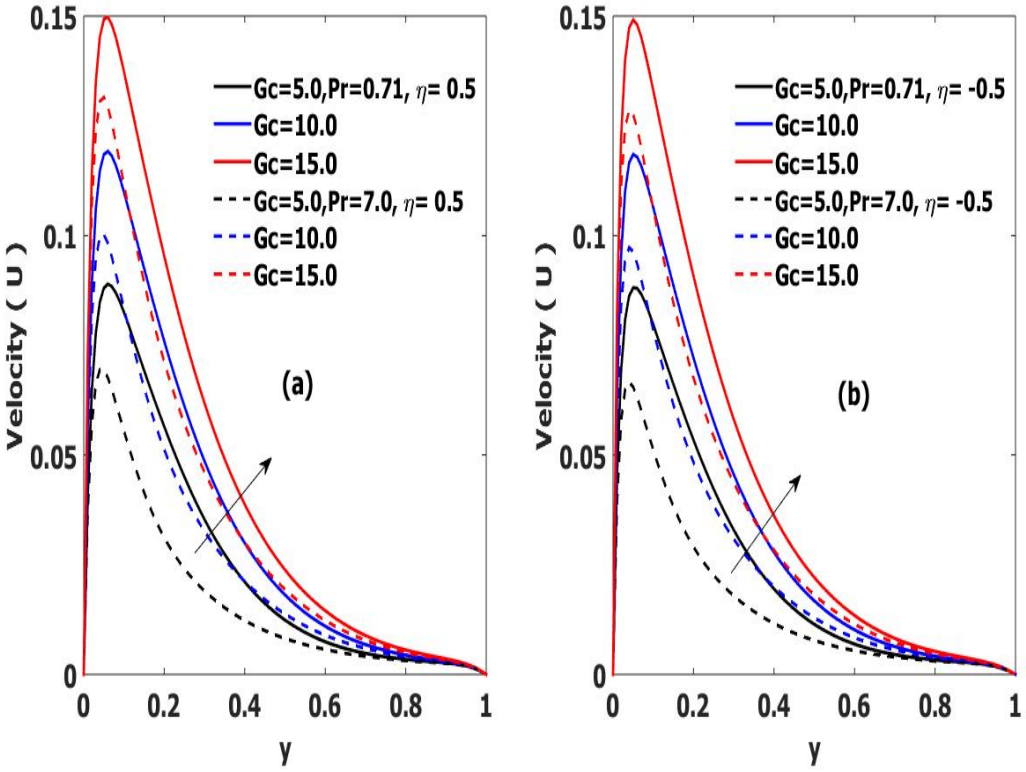

Figure 4: Influence of Gc on velocity profiles

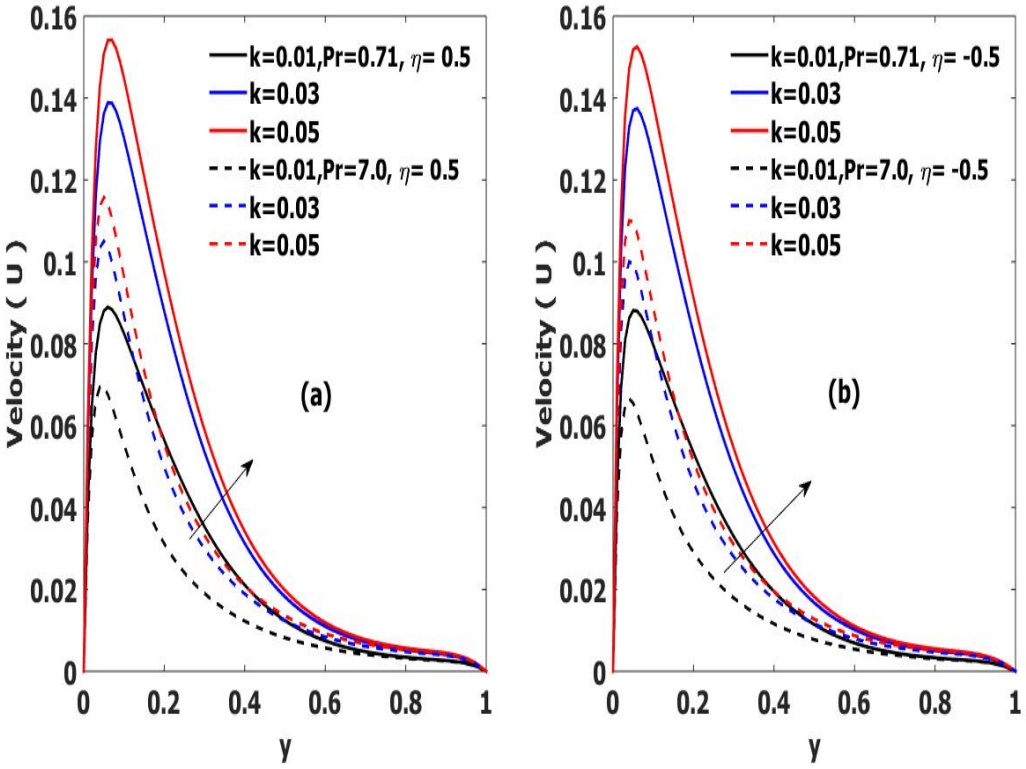

Figure 5: Influence of K on velocity profile

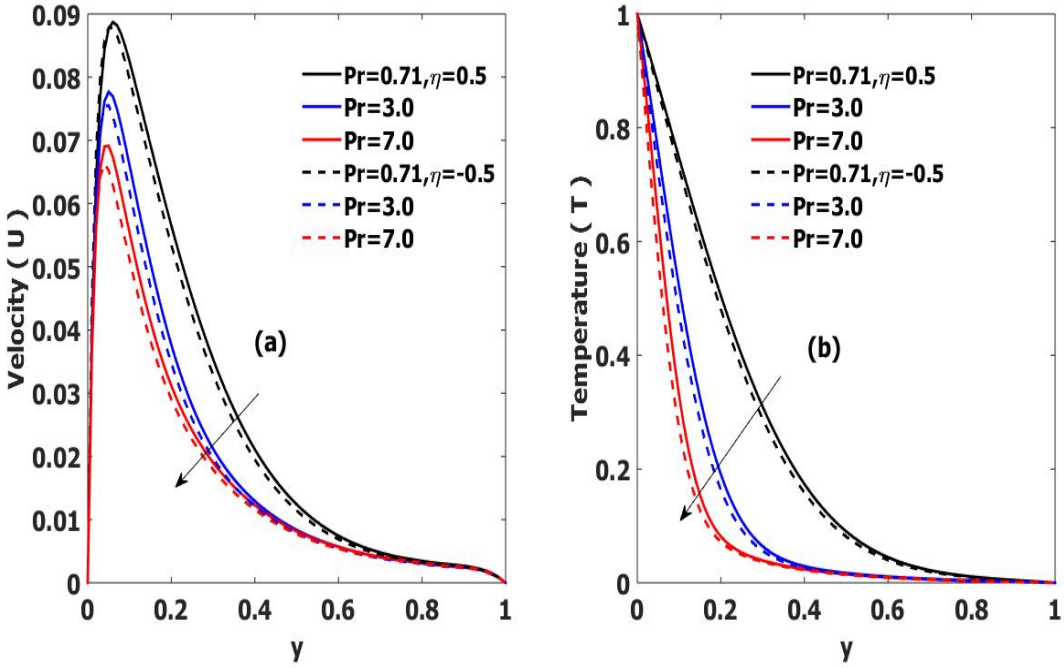

Figure 6: Influence of Pr on velocity and temperature profile

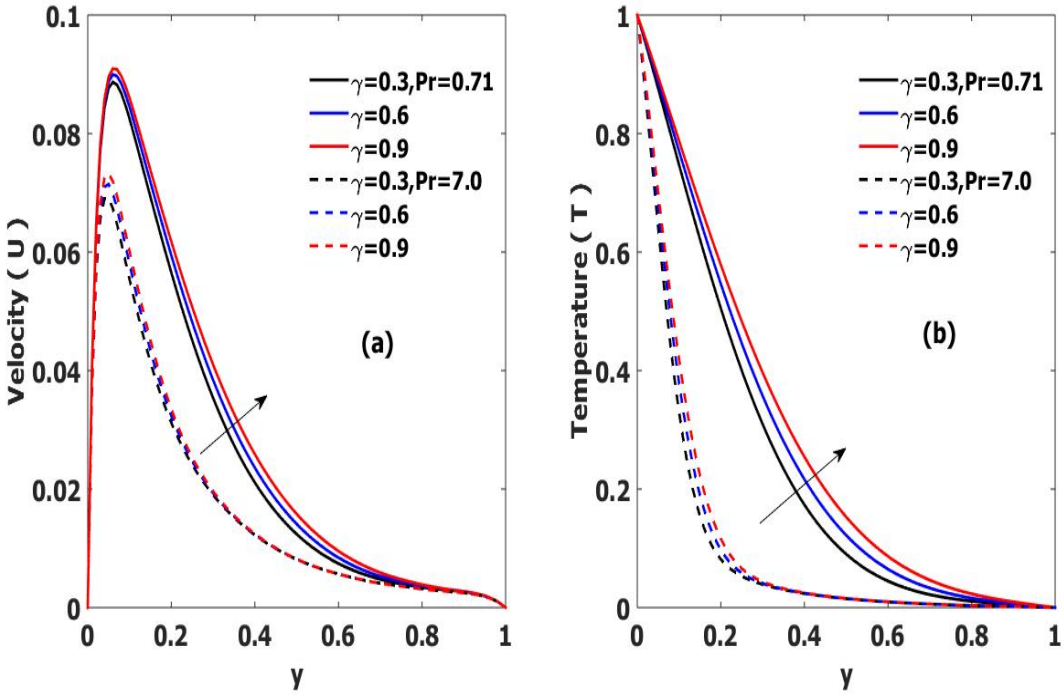

Figure 7: Influence of γ on velocity and temperature profiles

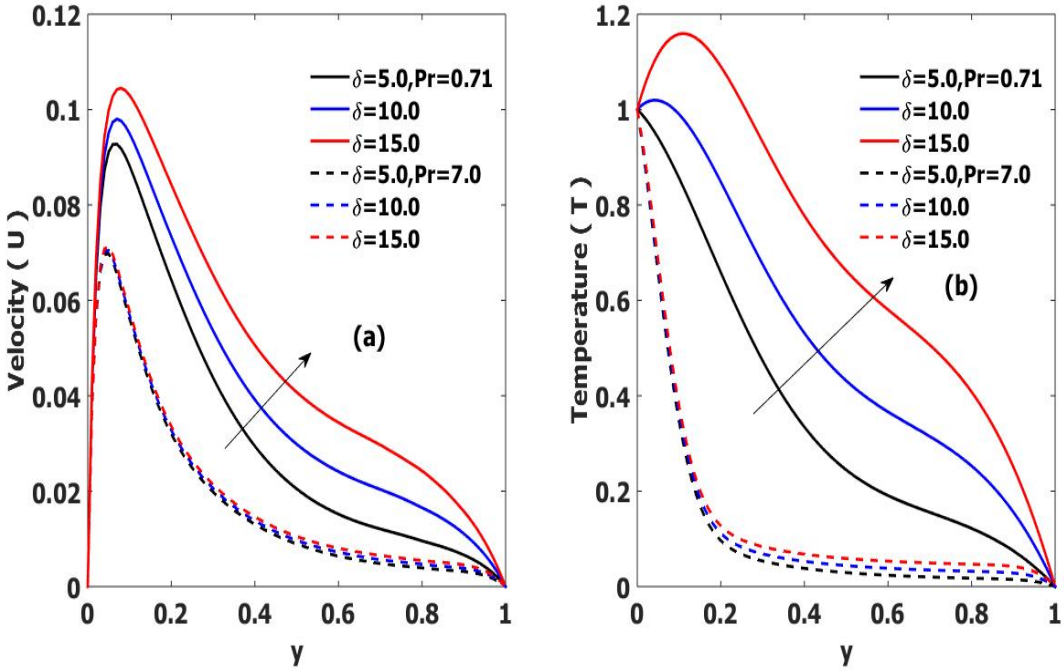

Figure 8: Influence of δ on velocity and temperature profiles

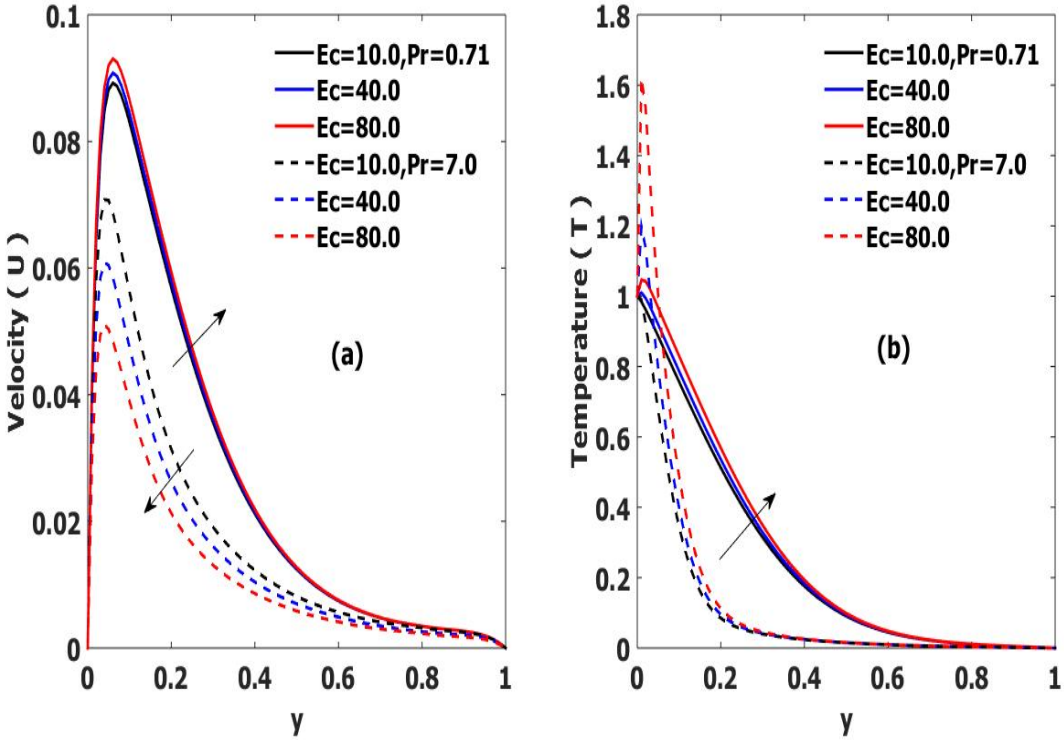

Figure 9: Influence of Ec on velocity and temperature profiles

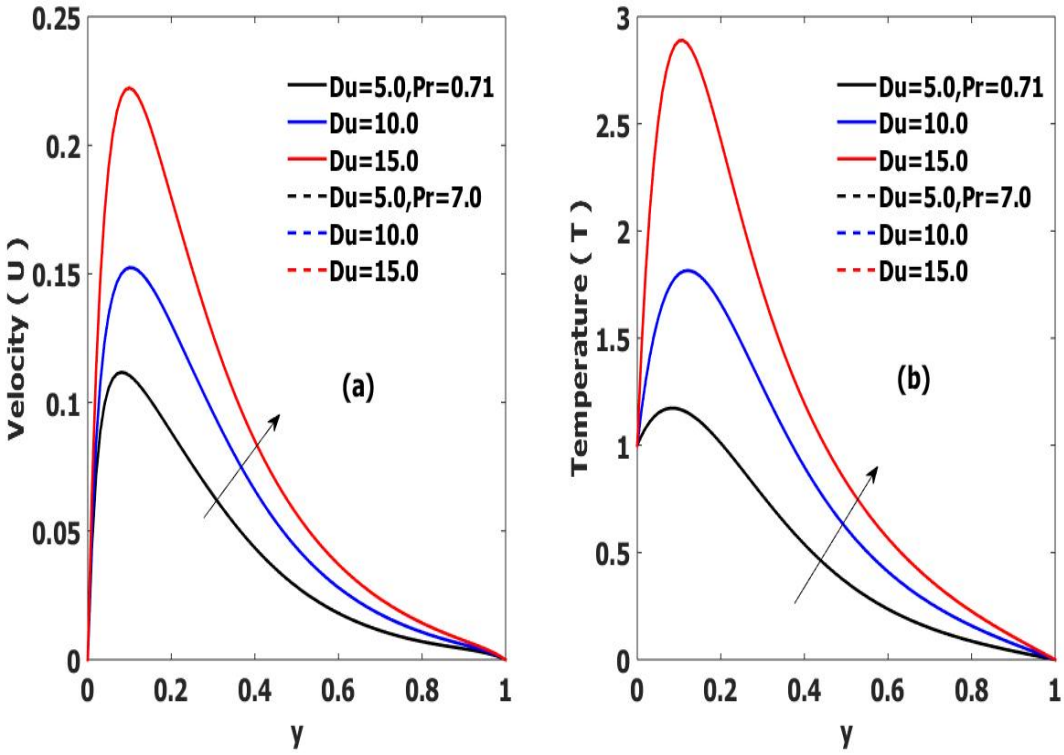

Figure 10: Influence of Du on velocity and temperature profiles

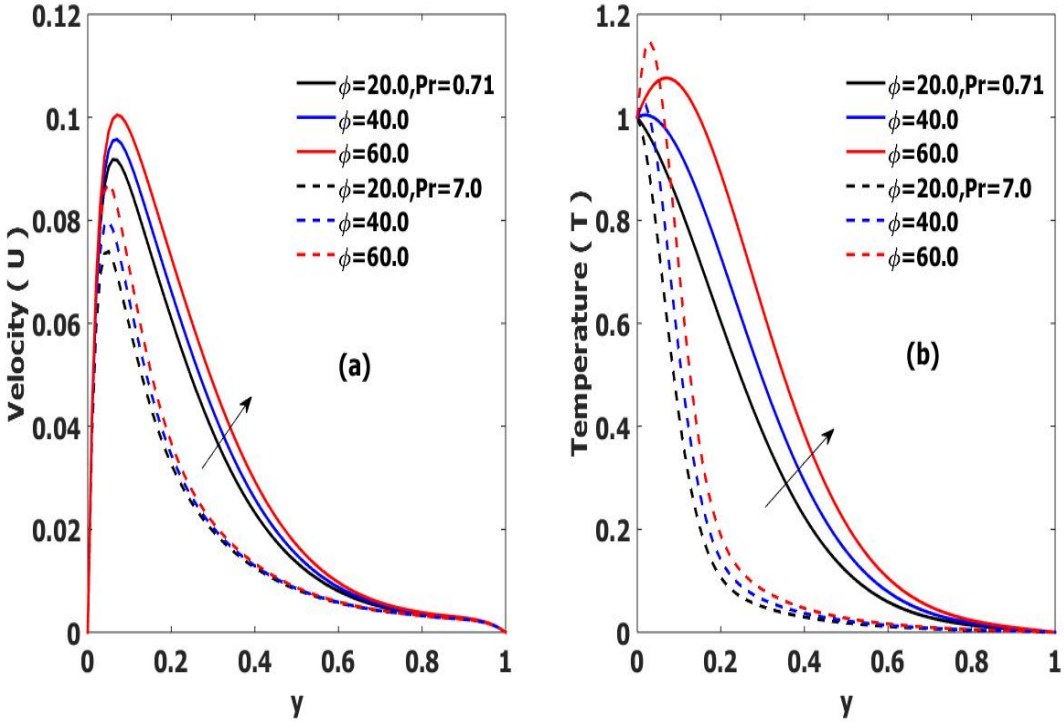

Figure 11: Influence of ϕ on velocity and temperature profiles

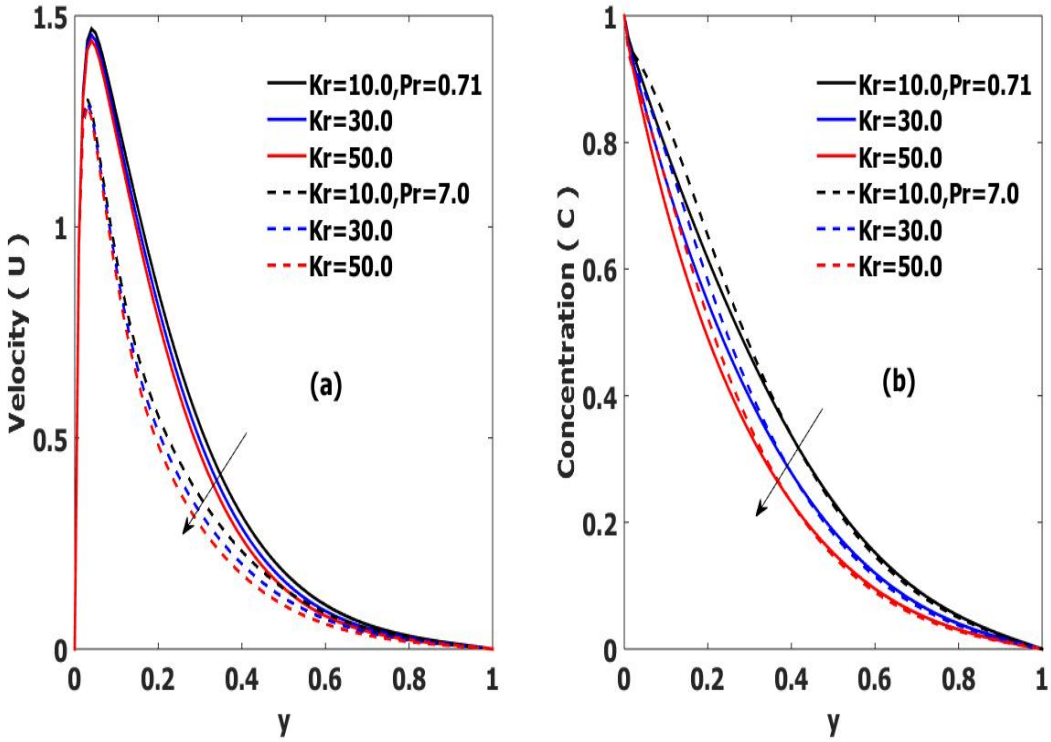

Figure 12: Influence of Kr on velocity and concentration profiles

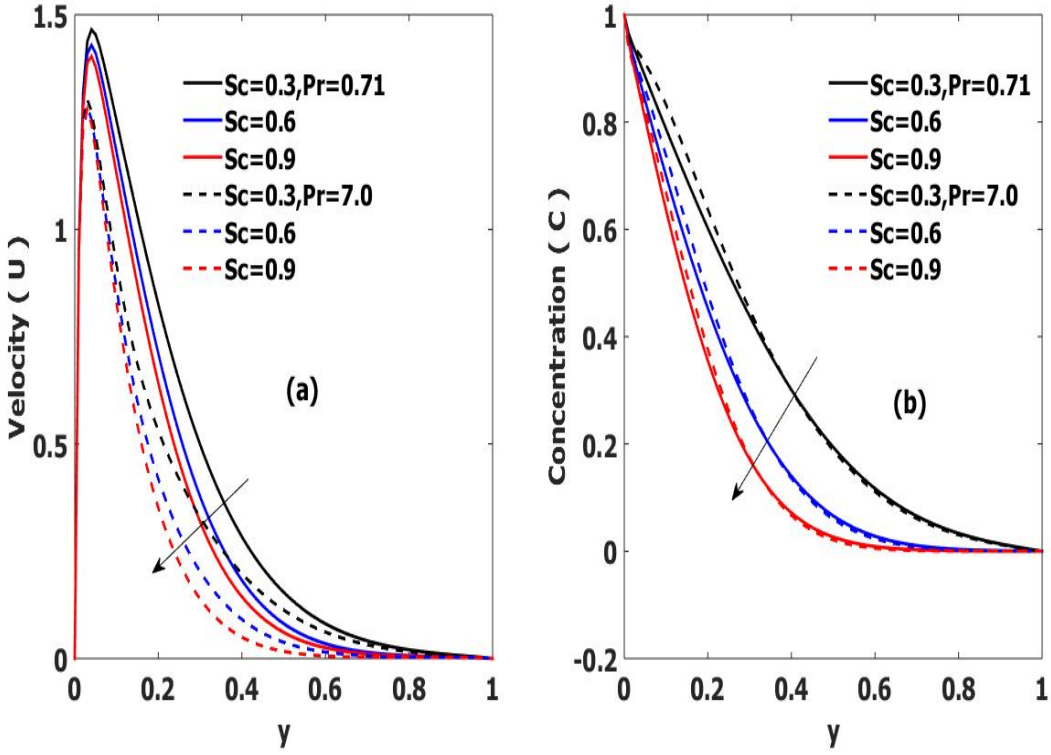

Figure 13: Influence of Sc on velocity and concentration profiles

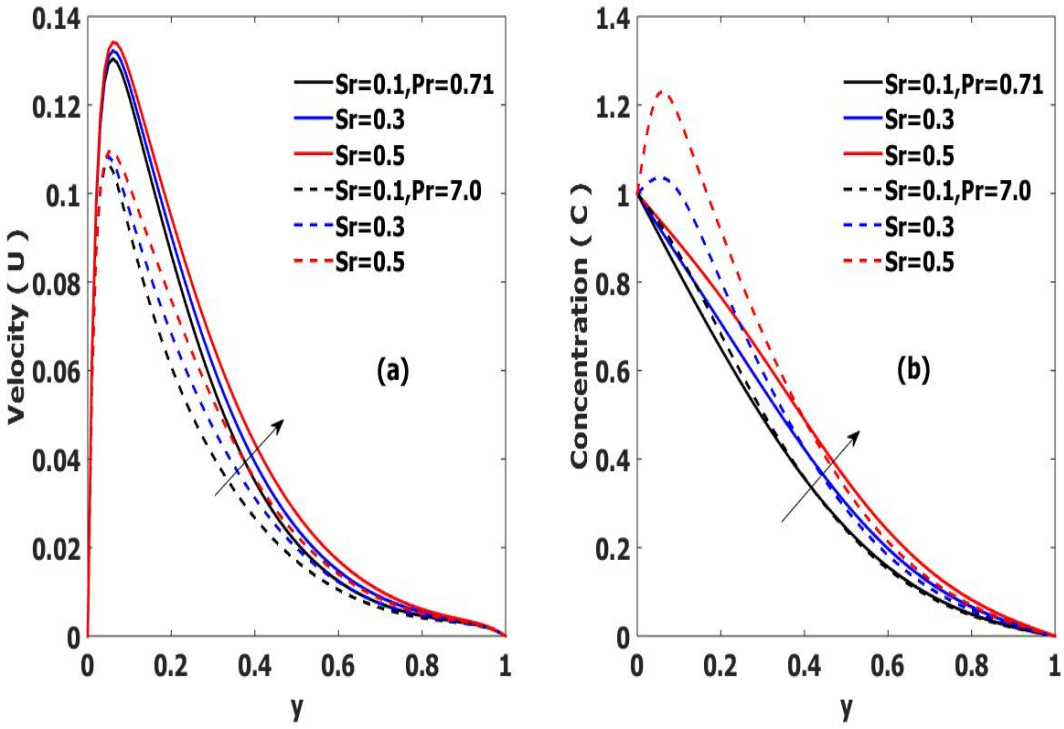

Figure 14: Influence of Sr on velocity and concentration profiles

The version in skin-friction coefficient, the rate of heat transfer in the kind of Nusselt number and the rate of mass transfer in the kind of Sherwood number for various parameters are analyzed through Tables 1–3. Skin friction coefficient decelerates with increasing magnetic parameter (M), Forchheimer parameter (Fr), Dufour number (Du) and Soret number (Sr); likewise it enhances thermal Grashof number (Gr), mass Grashof number (Gc), Eckert number (Ec),variable thermal conductivity parameter (γ) and Frank-Kamenetskii parameter (δ) (Table 1). The magnitude of the Nusselt number *Nu* increases with increasing Eckert number (Ec), activation energy parameter (ε), variable thermal conductivity parameter (γ), heat source parameter (ϕ), and Frank-Kamenetskii parameter (δ) (Table 2). In the same fashion, the magnitude of the Sherwood number *Sh gains* with growing Soret number (Sr) and dilutes with increasing Schmidt number (Sc) and chemical reaction (Kr). For the validity of our work, we have compared our results with the existing results.

Table 1: Values of the skin-friction for different parameters.

M	Gr	Gc	Fr	EC	Γ	δ	Du	Sr	Numerical Values of Skin Friction (Cf) for different values of Physical Parameters			
									n=1		n=2	
									SK0	SK1	SK0	SK1
1.0									$1.92127x10^2$	7.81038	5.31469	0.86510
2.0									$1.83698x10^2$	7.44146	5.21128	0.86510
3.0									$1.75757x10^2$	7.09584	5.11265	0.78743
	1.0								77.55436	7.48377	2.02419	0.36523
	3.0								90.01337	7.51399	2.36499	0.41502
	5.0								$1.02361x10^2$	7.54489	2.70657	0.46524
		1.0							$1.38957x10^2$	7.56436	3.61421	0.53990
		2.0							$1.44973x10^2$	7.59116	3.80253	0.57562
		3.0							$1.50961x10^2$	7.61809	3.99101	0.61147
			1.0						$1.92127x10^2$	7.81038	5.31469	0.86510
			2.0						$1.77849x10^2$	7.78288	5.27421	0.85682
			3.0						$1.65944x10^2$	7.75569	5.23512	0.84876
				0.1					$1.94271x10^2$	7.82351	5.32176	0.86771
				0.2					$1.96746x10^2$	7.83844	5.32965	0.87062
				0.3					$1.99325x10^2$	7.85375	5.33760	0.87354
					1.0				$1.92126x10^2$	7.81038	5.31469	0.86510
					2.0				$1.92168x10^2$	7.74973	5.18267	0.80431
					3.0				$1.90643x10^2$	7.70944	5.07395	0.76057
						0.1			$1.92127x10^2$	7.81038	5.31469	0.86510
						0.2			$1.92147x10^2$	7.82738	5.32344	0.87266
						0.3			$1.92167x10^2$	7.84443	5.33222	0.88025
							0.1		$1.92127x10^2$	7.81038	5.31469	0.86510
							0.2		$1.92231x10^2$	7.82958	5.34603	0.88264
							0.3		$1,92335x10^2$	7.84886	5.37746	0.90022
								0.01	$1.92127x10^2$	7.81037	5.31469	0.86510
								0.03	$1.92127x10^2$	7.81044	5.31477	0.86516
								0.05	$1.92127x10^2$	7,81056	5.31495	0.86526

Table 2: Values of the Nusselt number for different parameters.

Ec	ε	b	Du	γ	ϕ	δ	Numerical and Values of (Nu) Nusselt number for different values of Physical Parameters			
							n=1		n=2	
							SK0	SK1	SK0	SK1
0.1							-3.58650	0.36000	3.20982	0.26518
0.2							-7.85377	0.38994	3.16104	0.27210
0.3							-12.4155	0.42120	3.11188	0.27908
	0.01						0.02503	0.33409	3.25342	0.25901
	0.02						0.025142	0.33408	3.25347	0.25901
	0.03						0.02525	0.33408	3.25354	0.25901
		1.0					2.75997	0.31342	3.37088	0.20544
		3.0					2.20186	0.23798	3.34583	0.21681
		5.0					1.61753	0.26375	3.32019	0.22848
			0.1				0.02503	0.33409	3.25342	0.25901
			0.2				-0.04950	0.34761	3.20304	0.27085
			0.3				-0.12452	0.36123	3.15249	0.28276
				1.0			0.02503	0.33409	3.25342	0.25901
				2.0			1.14949	0.30676	3.18087	0.24379
				3.0			1.68657	0.28466	3.14672	0.23376
					1.0		0.02503	0.33409	3.25342	0.25901
					2.0		-0.03887	0.34481	3.21346	0.26734
					3.0		-0.10384	0.35600	3.17301	0.27602
						0.1	0.02503	0.33409	3.25342	0.25901
						0.2	0.00569	0.34514	3.24094	0.26924
						0.3	-0.01374	0.35624	3.22843	0.27951

Table 3: Values of the Sherwood number for different parameters.

Sc	Kr	Sr	Numerical Values of Sherwood number for different values of Physical Parameters			
			n=1		n=2	
			Sh0	Sh1	Sh0	Sh1
0.2			2.74946	0.36937	2.74940	0.36937
0.4			3.80788	0.17578	3.80778	0.17578
0.6			4.60947	0.09408	4.60933	0.09408
	1.0		3.25068	0.26137	3.25062	0.26137
	2.0		3.21688	0.26778	3.21682	0.26778
	3.0		3.18275	0.27439	3.18269	0.27439
		0.1	2.93644	0.32770	2.93016	0.32762
		0.2	2.94400	0.33030	2.91887	0.32998
		0.3	2.95664	0.33464	2.90003	0.33391

5. Conclusions

A non-Newtonian power-law fluid's MHD free convection flow across a vertical plate with variable thermal conductivity and suction/injection effects has been taken into account. The results of the mathematical analysis were concluded and compiled as follows:

1. The chemical reaction parameter and Schmidt number cause the concentration distribution to drop and the Soret number to rise
2. As the thermal Grashof number, mass Grashof number, and porosity parameter rise, the velocity rises as well.
3. The t velocity decreases as the magnetic field's strength increases.
4. Both the fluid velocity and the chemical reaction parameter decrease as the Schmidt number rises.
5. A decrease in temperature distribution is caused by an increase in the Prandtl number.
6. In accordance with the rising values of the heat source parameter, the velocity and dimensionless temperature are rising.
7. The skin friction coefficient reduces as the magnetic parameter increases, but it has the opposite effect when the Grashof numbers are heat or mass.
8. As Eckert's number and activation energy parameter increase, Nusselt's number also rises.
9. As Schmidt's number or chemical reaction parameter increases, Sherwood's number decreases, but Soret's parameter increases.

Acknowledgments

The writers are grateful for the financial support for this project from Sokoto State University, Sokoto, Nigeria, through Tertiary Education Trust Fund (Tetfund)

References

[1] S. Djukic Djordje, D. Vujanovic Bozidar, A variational principle for the two-dimensional boundary-layer flow of non-Newtonian power-law fluids, Rheological Acta 14 (10) (1975) 881–890.

[2] J.P. Pascal, H. Pascal, On some similarity solutions to shear flows of non-Newtonian power law fluids, Acta Mechanica 112(1994) 229–236.

[3] M. Kumari, H.S. Takhar, G. Nath, Non similar mixed convection flow of non-Newtonian fluid past a vertical edge, Acta Mechanica 113 (1995) 205–213.

[4] M. Kumari, I. Pop, H.S. Takhar, G. Nath, Free convection boundary layer flow of a non-Newtonian fluid along a vertical way surface, International Journal of Heat and Fluid Flow 18
(1997) 525–632.

[5] M.A. El-Hakiem, M.F. El-Amin, Mass transfer effects on then on-Newtonian fluids past a vertical plate embedded in a porous medium with non-uniform surface heat flux, Heat and Mass
Transfer 37 (2/3) (2001) 293–297.

[6] R.S.R. Gorla, H.S. Takhar, I. Pop, M. Kumari, A. Slaouli, Free convection power-law near dimensional stagnation point, International Journal of Heat and Fluid Flow 16 (1995) 62–68.

[7] Anderson HI, Bech KH, Dandapat BS. Magnetohydrodynamic flow of a power law fluid over a stretching sheet. Int J Non-Linear Mech 1992; 27:929–36.
[8] Chen CH. Effects of magnetic fields on suction/Injection on convection heat transfer of non-Newtonian power law fluids past a power law stretched sheet surface heat flux. Int J Ther Sci 2008; 47:954–61.
[9] Chaitanya NSK, Dhiman AK. Non-Newtonian power-law flow and heat transfer
across a pair of side-by-side circular cylinders. Int J Heat Mass Transfer 2012; 55:5941–58.
[10] Sui J, Zheng L, Zhang X, Chen G. Mixed convection heat transfer in power lawfluids over a moving conveyor along an inclined plate. Int J Heat Mass Transfer 2015; 85:1023–33.
[11] Yao S, Fang T, Zhong Y. Heat transfer of a generalized stretching/shrinking wall
problem with convective boundary conditions. Commun Nonlinear Sci Numer Simul 2011; 16:752–60.
[12] Makinde OD, Aziz A. Mixed convection from a vertical plate embedded inporous medium with convective boundary conditions. Int J Ther Sci 2010; 49:1813.
[13] Kan M, Malik R, Munir A. Mixed convective heat transfer to Sisko fluid over a radially stretching sheet in the presence of convective boundary conditions. AIP Adv 2015;5. http://dx.doi.org/10.1063/1.4929832. 087178.
[14] Mahanta G, Shaw S. 3D Casson fluid flow past a porous linearly stretching sheet with convective boundary condition. Alex Eng J 2015; 54:653–9.
[15] Hayat T, Iqbal Z, Qasim M, Obaidat S. Steady flow of an Eyring Powell fluid over a moving surface with convective boundary conditions. Int J Heat Mass Transfer 2012; 55:1817–22.
[16] Shahzad A, Ali R. MHD flow of a non-Newtonian power law fluid over a vertical stretching sheet with the convective boundary condition. Walai J Sci Tech 2012; 10:43–56.
[17] Sorbie, K. S., *Polymer-improved Oil Recovery*, Boca Raton, FL: CRC Press, 1991.
[18] Vajravelu K., Rollins D., Hydromagnetic flow of a second-grade fluid over a stretching sheet, Appl. Math. Comput., 2004, 148,
[19] Baag S., Acharya M.R., Dash G.C., Mishra S.R., MHD flow of avisco-elastic fluid through a porous medium between infinite parallel plates with time dependent suction, J. Hydrodyn., 2015, 27(5), 840-847.
[20] Reddy M.G., Rani M.V.V.N.L.S., Kumar K.G., Cattaneo-Christov heat flux and non-uniform heat-source/sink impacts on radiative Oldroyd-B two-phase flow across a cone/wedge, J. Braz.Soc. Mech. Sci. Eng., 2018, 40, 95.
[21] Gireesha B.J., Archana M., Prasannakumara B.C., R.S.R Gorla, O.D. Makinde, MHD three-dimensional double diffusive flow of Casson nanofluid with buoyancy forces and nonlinear thermal radiation over a stretching surface, Int. J. Numer. Meth. Heat Fluid Flow, 2017, 27(12), 28.
[22] Gireesha B.J., Prasannakumara B.C., Gorla R.S.R., Thermal radiation and chemical reaction effects on boundary layer slip flow and melting heat transfer of nanofluid induced by a nonlinear stretching sheet, Nonlin. Eng., 2016, 5(3), 147-159.
[23] Mahantesh M. Nandeppanavar, Vajeravelu K., Abel M.S., Siddalingappa M.N., MHD flow and heat transfer over a stretching surface with variable thermal conductivity and partial slip,
Meccanica, 2017, 48(6), 1451-1464.
[24] Abel M., Siddheshwar P.G., Mahantesh M., Nandeppanavar, Heat transfer in a viscoelastic boundary layer flow over astretching sheet with viscous dissipation and non-uniform heat source, International Journal of Heat and Mass Transfer, 50 (5-6) (2007) 960-966.
[25] Mahantesh M. Nandeppanavar, K. Vajravelu, M.S. Abel, Heat transfer in MHD viscoelastic boundary layer flow over a stretching sheet with thermal radiation and non-uniform heat source/sink, Communications in Nonlinear Science and Numerical Simulation, 2011, 16(9), 3578-3590.